MOLYBDENUM DISULFIDE NANOPOROUS MEMBRANES FOR WATER DESALINATION

BY

MOHAMMAD HEIRANIAN

THESIS

Submitted in partial fulfillment of the requirements
for the degree of Master of Science in Theoretical and Applied Mechanics
in the Graduate College of the
University of Illinois at Urbana-Champaign, 2016

Urbana, Illinois

Adviser:

Professor Narayana R. Aluru

Abstract

We demonstrate molybdenum disulfide (MoS_2) as a nano porous membrane for water desalination. By performing extensive molecular dynamics simulations, we find that a nanopore in a single-layer MoS_2 can effectively reject salt ions and allow transport of water at a high rate. More than 88% of ions are rejected by membranes having pore areas ranging from 20 to 60 $Å^2$. Water flux through the nanoporous MoS_2 membrane is found to be 2 to 5 orders of magnitude greater than that of other known nanoporous membranes (MFI-type zeolite, commercial polymeric seawater Reverse Osmosis (RO), brackish RO, Nanofiltration and High-flux RO). Pore chemistry and architecture are shown to play a significant role in modulating the water flux. MoS_2 pores with only molybdenum atoms on their edges give rise to higher fluxes which are about 70% greater than that of graphene nanopores. These observations are explained by the permeation coefficients, energy barriers, water density and velocity distributions in the pores. Our findings pave way towards identifying efficient membranes for water desalination.

Keywords: Water Desalination, Single-Layer MoS_2, Nanopores, Graphene, Hourglass nanopore, Nanofluidics, Transition Metal Dichalcogenide

To my family and friends

Acknowledgments

I would like to gratefully thank my adviser, Professor Narayana R. Aluru, for his great supervision and guidance. Nothing could have been achieved without his critical and scientific assessment of the work. I also appreciate the time, encouragement and support he has always offered me throughout my research project. I also need to thank Amir Barati Farimani for patiently answering my questions and sharing his helpful insights.

I would like to acknowledge the financial support by AFOSR under grant # FA9550-12-1-0464, and NSF under grants 1264282, 1420882 and 1506619 and the Beckman Institute for Advanced Science and Technology. I also need to acknowledge the use of the parallel computing resource Blue Waters provided by the University of Illinois and National Center for Supercomputing Applications (NCSA).

I am deeply thankful to my loving and supporting parents. Their unconditional love and support have always kept me advancing towards my goals. Finally, I would like to thank my uncle for the tremendous support he provides on my educational journey.

TABLE OF CONTENTS

CHAPTER 1

INTRODUCTION

1.1 Water Desalination Using Nanoporous Membranes

Producing fresh water is currently a great challenge facing the society.[1-4] High capital costs and low efficiency of current desalination technology motivate the need for advances in desalination technology.[5,6] Approximately, half of the current desalination plants use Reverse Osmosis (RO) technologies.[2,5] RO based on traditional polymeric membranes faces several challenges including slow water transport.[7,8] Advances in nanotechnology open up opportunities to design energy-efficient membranes for water desalination.[9,10] Nanopores with diameters ranging from a few Angstroms to several nanometers can be drilled in membranes to fabricate molecular sieves.[11-13] As the diameter of the nanopore approaches the size of the hydrated ions, various types of ions can be rejected by nanoporous membranes promising efficient water desalination. Among nanoscale materials, graphene and carbon nanotubes were extensively studied for both water transport and desalination.[14-18] Graphene, a single-atom thick membrane (0.34 nm), was demonstrated to have several orders of magnitude higher flux rates compared to conventional zeolite membranes.[6,11,15,16,19,20] Since water flux through a membrane scales inversely with the membrane's thickness,[11] graphene is attractive over most other materials due to its single-atom thickness.[12,16]

It has been shown that chemical functionalization of a graphene nanopore (e.g., adding hydroxyl groups) can enhance its permeability,[19,20] but reduces desalination efficiency.[19] Hydroxyl groups provide hydrophilic sites at the edge of the pore, which give rise to the attraction of water molecules and enhanced flux due to denser packing of water inside the pore.[19] Adding precise functional groups to the edge of nanopores requires complex fabrication[21]; therefore, identifying a single-atom thick membrane with hydrophilic sites can lead to further advances in water desalination technology.

1.2 Motivation: Molybdenum Disulfide (MoS_2)

Recently, a nanopore in a single-layer MoS_2 has been investigated for DNA sequencing and has been shown to provide better results compared to graphene nanopores.[9,22] Compared to graphene, a MoS_2 single-layer has two types of atoms, *i.e.* molybdenum (Mo) and sulfur (S). One layer of molybdenum atoms is sandwiched between two layers of sulfur atoms. A single-layer MoS_2 has a thickness of about 1.0 nm [23] and is a mechanically strong material with an effective Young's modulus of 270 +/- 100 GPa, that is comparable to that of steel.[24] The possibility to craft the pore edge with Mo, S or both provides flexibility to design the nanopore with desired functionality. Recently, it has been shown that a nozzle-like structure of protein channels and other nanoscale membranes enhances water permeation.[25] The fish-bone structure of MoS_2 makes it amenable for a nozzle-like sub-nanometer pore for fast water permeation.[25] The combination of membrane's thinness, pore geometry and chemistry in a single-layer MoS_2 can lead to enhanced flux and efficiency.

1.3 Experimental Studies on Fabrication and Manufacturability of MoS_2 Membranes

Although theoretical studies of membrane efficiency are important in desalination technology, there are other aspects concerning fabrication and manufacturability of membranes such as large-area synthesis with defect-free, well-defined sealed membranes and precise pore generation that need to be addressed. Using a highly focused electron beam, and transmission electron microscope (TEM), versatile nanopores with diameters ranging from 1-10 nm were sculpted successfully in MoS_2 membranes.[9] Waduge *et al.*[26] reported that a large area, well-sealed membrane with nanopores as tiny as 2.8 nm can be fabricated. Compared to graphene, the contamination of these membranes can be lower as carbon atoms in graphene are more susceptible to contamination during chemical vapor deposition (CVD) growth. Feng *et al.*[27] also achieved high quality scalable fabrication of nanopores in a single-layer MoS_2 with sub-nanometer precision using electrochemical reaction (ECR). Several other studies have been performed on the synthesis of large-area MoS_2 monolayers.[28-37] Recently, a few groups[29,34,37] have successfully used CVD to produce highly crystalline MoS_2 of centimeter dimensions. In another study[36], a refined CVD method was proposed to create high-quality monolayer MoS_2 crystals in which the grain boundaries of MoS_2 were faceted more strongly than that of graphene resulting in mechanically more stable MoS_2 monolayers. Membrane sealing also plays an essential role in synthesis of large-area membranes required in desalination. Waduge *et al.*[26] showed that their CVD approach resulted in almost fully sealed MoS_2 membranes. Combination of these results[9,13,26-37] and the recent focus on single layer MoS_2 fabrication is promising for the large scale manufacturing of a single-layer MoS_2.

In the next chapters, we demonstrate that a single-layer MoS_2 can effectively separate ions from water. Using molecular dynamics simulations (MD), we investigate water desalination in MoS_2 as a function of pore size, chemistry, geometry and applied hydrostatic pressure.

CHAPTER 2

SIMULATION METHODS

2.1 Molecular Dynamics Simulations

Molecular dynamics simulations are governed by the classical Newton's law of motion. For a system of N particles, knowing the position, $r_{j,}$ and velocity, $v_{j,}$ of each particle j defines the state of the system at any time (t). To obtain the trajectories of all particles in time, the equation of motion (equation 2.1) is integrated provided that the information about the force (F_j) on each particle with mass, m_j, is known. At any time, the forces can be computed from a potential function (U) which is called the force field (see equation 2.2 and section 2.3).

$$m_j \frac{\partial^2 r_j}{\partial t^2} = F_j \,, \;\; j = 1 \ldots N \tag{2.1}$$

$$F_j = -\frac{\partial U}{\partial r_j} \tag{2.2}$$

In molecular dynamics, the most popular time integrator is the Verlet algorithm. It has gained its popularity because of its stability and accuracy (fourth order accurate in time). The updated positions is obtained from the following time advancement algorithm:

$$\boldsymbol{r}(t + \Delta t) = 2\boldsymbol{r}(t) - \boldsymbol{r}(t - \Delta t) + \frac{\boldsymbol{F}(t)}{m}\Delta t^2 + O(\Delta t^4) \tag{2.3}$$

where Δt is the time step used in the simulations. The velocities can be obtained from a central difference operator scheme (see equation 2.4). However, this scheme is second-order accurate

which results in lower accuracies in calculations of velocities. One way to overcome this inaccuracy is to use the so called velocity Verlet algorithm where positions, velocities and forces are computed at every updated time.

$$\boldsymbol{v}(t) = \frac{\boldsymbol{r}(t+\Delta t)-\boldsymbol{r}(t-\Delta t)}{2\Delta t} \tag{2.4}$$

2.2 Simulation System Setup

Molecular Dynamics simulations were performed using the LAMMPS package[38]. The graphene sheet, which acts as a rigid piston to exert external pressure on saline water, along with the MoS_2 sheet, water molecules and ions were created by the Visual Molecular Dynamics (VMD).[39] The saline water box was placed between the graphene and MoS_2 sheet, and pure water was added on the other side of the MoS_2 sheet as shown in Fig. 1. Here, three pore edge types for MoS2 are considered to study the effect of terminating atoms and pore chemistry on the rate of water permeation and ion rejection. The first type of pore, which is labeled as Mixed in this study, is a combination of molybdenum and sulfur atoms. The other two pore types are labeled as Mo-only and S-only as these are terminated by molybdenum and sulfur atoms, respectively (Fig. 1b). A nanopore was drilled in MoS_2 by removing the desired atoms. The accessible pore areas considered range from 20 to 60 $Å^2$. The system dimensions are 4nm × 4nm × 13nm in x, y and z, respectively. The box contains about 16,000 atoms and the ions (sodium and chloride) have a molarity of ~1.0 which is higher than the usual salinity of seawater (0.599 M) because of the computational cost associated with low salinity solutions.

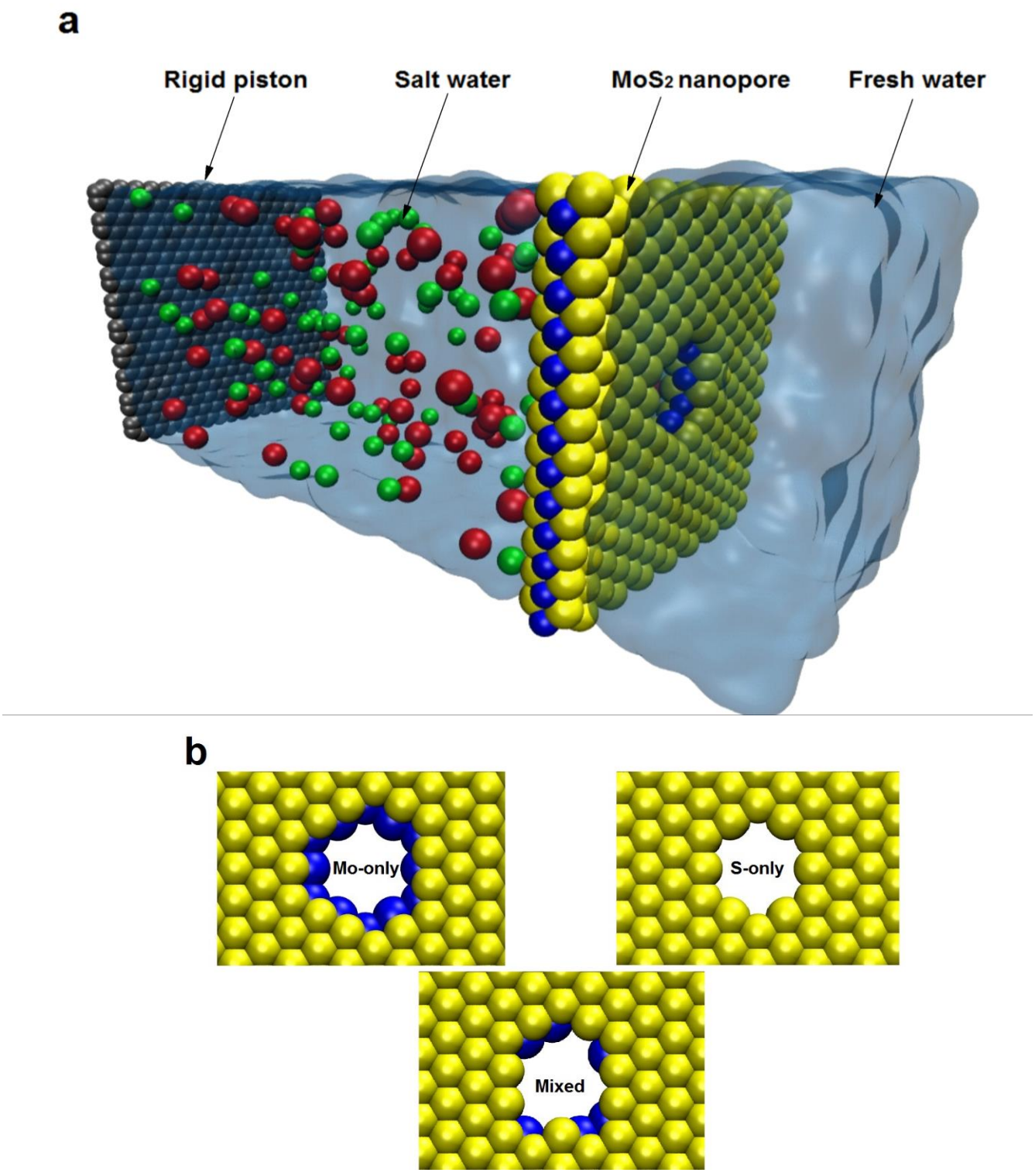

Figure 1 | (**a**) Schematic of the simulation box consisting of a MoS_2 sheet (molybdenum in blue and sulfur in yellow), water (transparent blue), ions (in red and green) and a graphene sheet (in grey). (**b**) Left: Mo-only pore type. Right: S-only pore type. Bottom: Mixed pore type.

The pore area, which is accessible to water molecules, is computed by considering the size of the atoms on the edge of each pore. First, the coordinates of all terminating atoms' centers as well as the van der Waals radii of sulfur and molybdenum are input into the SolidWorks program as shown in Fig. 2a. Then the accessible area is extruded through the atoms (Fig. 2b) and the pore area is calculated.

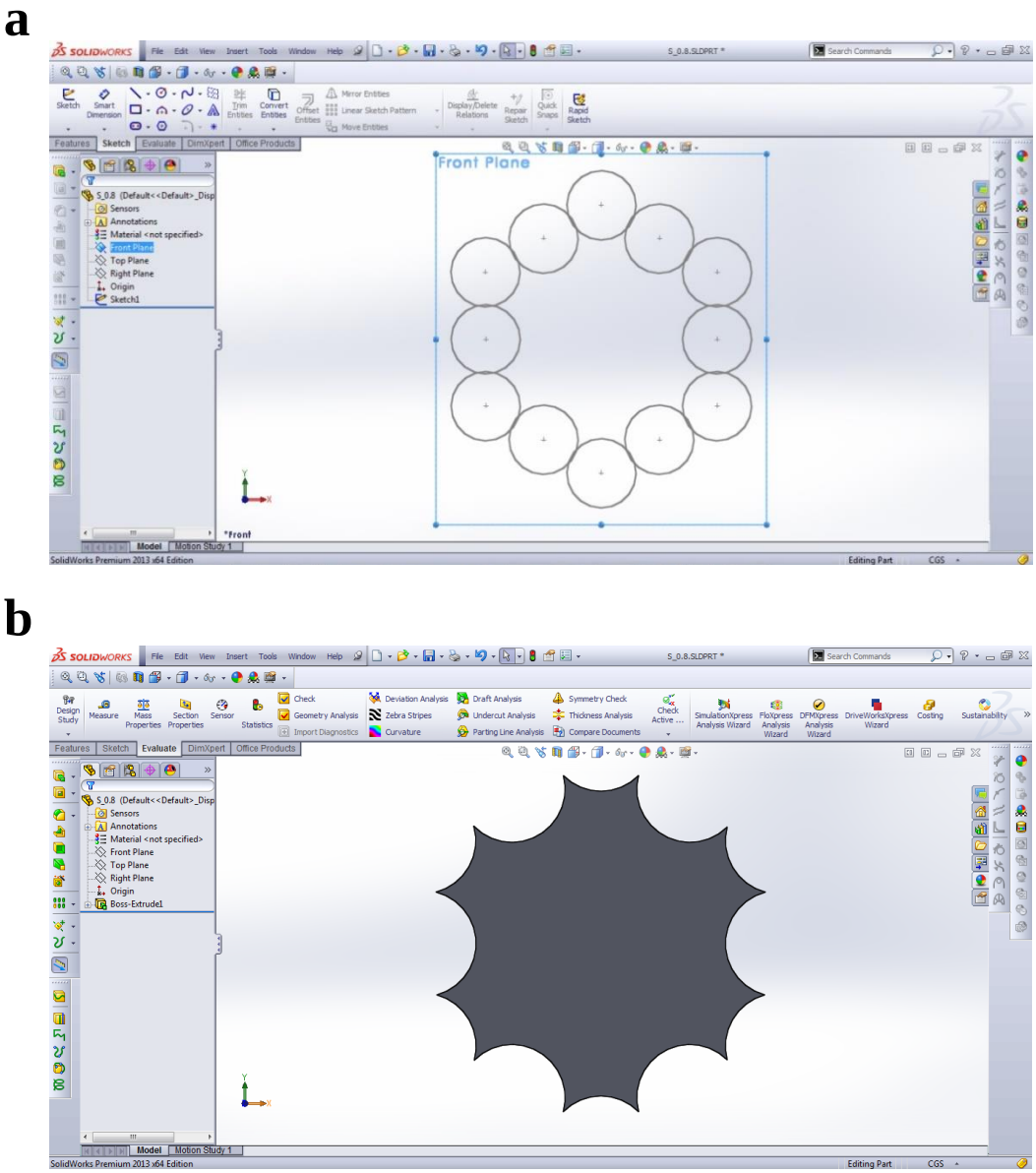

Figure 2 | (**a**) Terminating atoms of a pore represented by their size. (**b**) Extruded area of the pore.

The long range electrostatic interactions were calculated by the Particle Particle Particle Mesh (PPPM).[40] Periodic boundary conditions were applied in all the three directions. For each simulation, first the energy of the system was minimized for 10000 steps. Next, the system was equilibrated in NPT (constant number of particles, pressure and temperature) ensemble for 1 ns at a pressure of 1 atm and a temperature of 300 K. Graphene and MoS_2 atoms were held fixed in space during equilibration and the NPT simulations allow water to reach its equilibrium density (1 g cm^{-3}). Then, an additional NVT (constant number of particles, volume and temperature) simulation was performed for 2 ns to further equilibrate the system. Temperature was maintained at 300 K by using the Nosè-Hoover thermostat with a time constant of 0.1 ps.[41,42] Finally, the production non-equilibrium simulations were carried out in NVT ensemble for 10 ns where different external pressures were applied on the rigid graphene sheet (no longer frozen in space) to characterize the water filtration through the MoS_2 nanopores. In the production runs, the MoS_2 atoms were again held fixed in space to study solely the water transport and ion rejection properties of MoS_2. To accelerate the MD simulations and gather enough statistics in the 10-ns simulations, high external pressures ranging from 50 to 350 MPa were considered in this work. Trajectories of atoms were collected every picosecond to obtain the results. For accurate velocity calculations, however, the trajectories were dumped every femtosecond and the data was averaged over 25 sets of simulations with different initial thermal velocity distributions

2.3 Force Fields

As mentioned in section 2.1, the forces on particles need to be computed from some potential function which consists of non-bonded and bonded terms (see equation 2.5). The non-bonded

terms involve the van der Waals (vdW) and electrostatic interactions between each pair of atoms. The bonded terms account for bond, angle and dihedral interactions within a molecule.

$$U_{total} = U_{vdW} + U_{elec} + U_{bond} + U_{angle} + U_{dihedral} \tag{2.5}$$

The vdW interactions are modeled by a common 6-12 potential form of Lennard-Jones (LJ):

$$U_{LJ}(r_{ij}) = 4\varepsilon_{ij}\left[\left(\frac{\sigma_{ij}}{r_{ij}}\right)^{12} - \left(\frac{\sigma_{ij}}{r_{ij}}\right)^{6}\right] \tag{2.6}$$

where ε_{ij} and σ_{ij} are the minimum energy in the potential well and separation distance between two particles *i* and *j* where the energy is zero, respectively.

The electrostatic interactions are represented by the Coulombic potential:

$$U_{elec}(r_{ij}) = \frac{1}{4\pi\varepsilon_o}\frac{q_i\, q_j}{r_{ij}} \tag{2.7}$$

where ε_o, q_i and q_j are the permittivity of space, charge of particle *i* and *j*, respectively. These interactions are long range; therefore, they require robust computational schemes such as PPPM as discussed in the previous section.

Since the membrane atoms are frozen space, the bonded interactions are turned off for MoS_2. The SPC/E water model was used and the SHAKE algorithm was employed to maintain the rigidity of the water molecule. For non-bonded interactions, the mixing rule (Lorentz-Berthelot) was used to obtain the LJ parameters except for carbon-water interactions which were modeled by the force field parameters given in ref. 43. The LJ parameters are tabulated in Table 1. The LJ cutoff distance was 12 Å.

Table 1 | The Lennard-Jones parameters employed in the simulations are tabulated below.

Interaction	σ [Å]	ϵ [kcal mol^{-1}]
C-C[44]	3.3900	0.0692
Mo-Mo[45]	4.2000	0.0135
S-S[45]	3.1300	0.4612
O-O[44]	3.1656	0.1554
H-H[44]	0.0000	0.0000
Na-Na[46]	2.1600	0.3526
Cl-Cl[46]	4.8305	0.0128
C-O[43]	3.4360	0.0850
C-H[43]	2.6900	0.0383
Rest	Obtained by Lorentz-Berthelot rules.	

CHAPTER 3

RESULTS

3.1 Water Fluxes

Water fluxes through various MoS_2 nanopores as a function of the applied pressure gradient are presented in Fig. 3. Three MoS_2 pore types (Mixed, Mo-only and S-only) were studied to explore their rejection rate and flux. In order to investigate the relative performance of MoS_2 over other 2D materials, a graphene nanopore which has been shown to be promising for water desalination, is also considered.[11,19] For the sake of comparison, the three MoS_2 pores and the graphene pore have approximately equivalent accessible pore areas (Mixed, A=55.45 $Å^2$, Mo-only, A=56.42 $Å^2$, S-only, A=57.38 $Å^2$ and graphene, A=59.67 $Å^2$). Our results indicate that the Mo-only pore has the highest rate of water permeation followed by the Mixed, S-only and the graphene pore for all the applied pressures (Fig. 3). Water flux through the Mixed pore is intermediary between Mo-only and S-only nanopores. The higher water fluxes through MoS_2 nanopores compared to graphene nanopores imply that for a desired water flux a smaller applied pressure is needed with MoS_2 nanopores. Later, in this work, we will explain the physical chemistry and geometrical foundations of MoS_2 pore that give rise to higher flux.

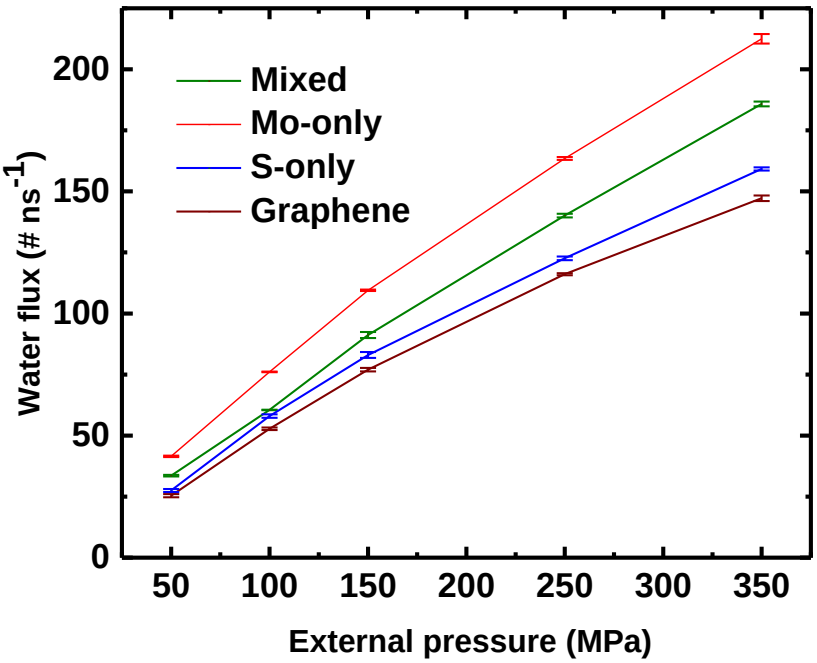

Figure 3 | Water flux as a function of the applied pressure for Mixed, Mo-only, S-only and graphene nanopores with equivalent pore areas.

3.2 Salt Rejection Efficiency

The other important aspect in water desalination is the ability of the membrane to reject ions. The percentage of total ions rejected by the MoS_2 and graphene pores are plotted as a function of the applied pressure in Fig. 4. The rejection is calculated after 1700 water molecules have filtered through the pores for all pressures. Pore sizes ranging from 20 to 60 $Å^2$ are considered for the three types of MoS_2 pores. The ion rejection decreases at higher pressures as high pressures induce higher forces on the ions giving rise to more ion translocation events. The ion rejection of small pores (e.g. 18.02 $Å^2$) is found to be 100% for all types of pores. For larger pore sizes, ions escape through the pore reducing the rejection efficiency. For the pores with equivalent areas (Mixed, A=55.45 $Å^2$, Mo-only, A=56.42 $Å^2$, S-only, A=57.38 $Å^2$ and graphene, A=59.67 $Å^2$), the general trend for ion rejection is quite similar regardless of the type of the pore (Fig. 4). In other words,

ion rejection is mainly dependent on the pore area and the type of the pore plays a less important role, e.g. for the four pores considered, the difference in rejection is less than 10% even at a high pressure of 350 MPa.

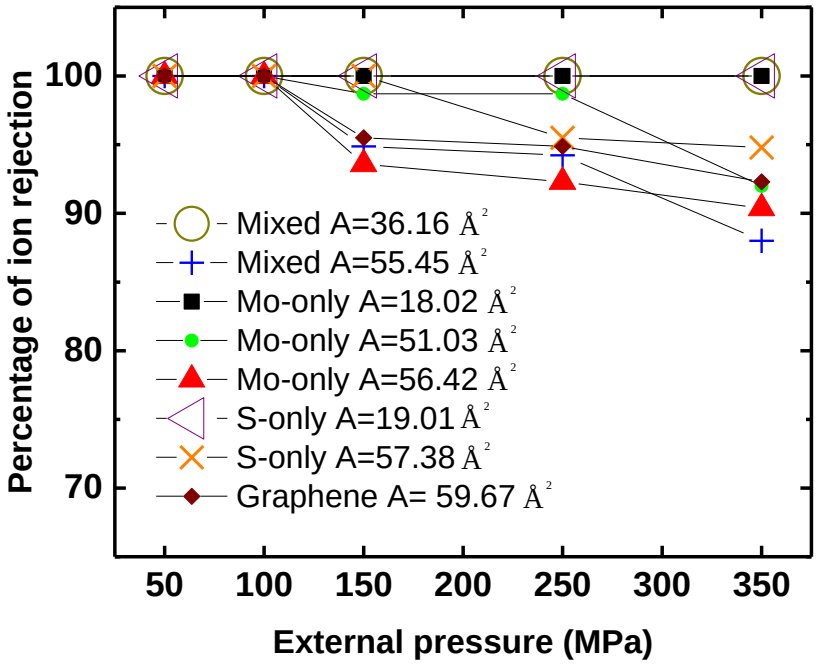

Figure 4 | Percentage of ion rejection by various pores as a function of the applied pressure. Pores with different edge chemistries as well as various pore areas (denoted by *A*) are considered.

As shown in Fig. 5, the water filtration rate increases sharply as the pore area increases from ~20 to ~50 $Å^2$. The sharp change in the water flow rate is due to the formation of single-file chain of water in small pores (~20 $Å^2$). As shown in ref. 11, the water flow rate is considerably reduced because of the weak hydrogen-bonding in single-file chains. For efficient water desalination, pore sizes should be chosen such that both the ion rejection and water filtration rate are optimized since very small pores lack high permeation rates and large pores (wider than 60 $Å^2$) fail to effectively reject ions.

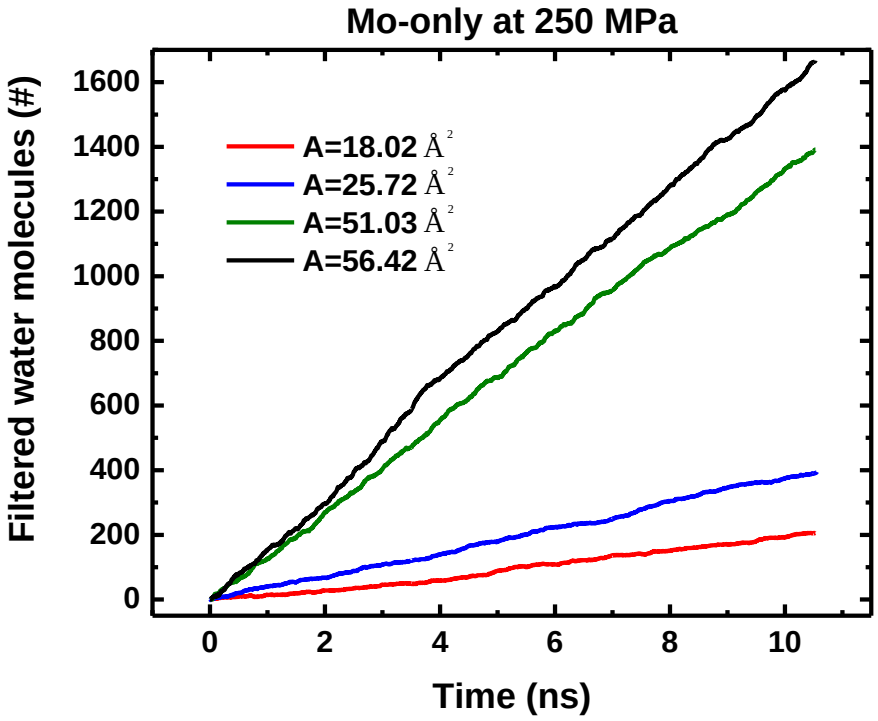

Figure 5 | Number of water molecules filtered through Mo-only pores as a function of simulation time for different pore areas at a fixed pressure of 250 MPa.

As observed by Cohen-Tangui *et al.*[19] for graphene, the polarizability of water also has a little effect on ion rejection in MoS_2 nanopores. To introduce the effect of polarization, the flexible SPC/F model[47] was used. The ion rejection percentages associated with the flexible water model are within 2% of those modeled with the SPC/E water.

3.3 Permeation Coefficient

To quantify the water permeability through various pores, we compute the permeability coefficient, *p*, across the pore. For dilute solutions,[48]

$$p = \frac{J_w}{-V_w \Delta C_s + \frac{V_w}{N_A k_B T} \Delta P} \quad (3)$$

where J_w is the flux of water (# ns^{-1}), V_w is the molar volume of water (18.91 mL mol^{-1}), ΔC_s is the concentration gradient of the solute (1.0 M), N_A is the Avogadro number, k_B is the Boltzmann constant, T is the temperature (300 K) and ΔP is the applied hydrodynamic pressure (MPa). The permeability coefficients of the Mixed, Mo-only, S-only and graphene pores were calculated to be 71.64 # ns^{-1}, 83.61 # ns^{-1}, 62.69 # ns^{-1} and 59.32 # ns^{-1}, respectively. These coefficients are expected to also hold true for small applied pressures (less than 10 MPa), which are normally used in water desalination, since the relationship between the external pressure and the rate of water permeation is observed to be quite linear (Fig. 3). Previous studies[49, 50] also show that water flux in small nanochannels is linear with respect to external pressure.

3.4 Energy Barrier

To calculate the energy barrier experienced by a water molecule when moving across a pore, the simulation box is first divided into bins of equal length along the axis of the pore (z). Next, in each bin, the force on each water molecule is averaged over both the simulation time and all the water molecules of the bin when the system is in equilibrium (no external pressure). Using the resulting average force (F) along the pore axis (z) (Fig. 6a), the energy required to move a water molecule from a reference point (z_o) in the bulk water to any other point (z) can be obtained by $\int_{z_0}^{z} F(z)dz$.

These barriers were computed to be $\Delta E_{\text{Mo-only}} = 8.50\ k_B T$, $\Delta E_{\text{Mixed}} = 8.84\ k_B T$, $\Delta E_{\text{S-only}} = 9.01\ k_B T$, $\Delta E_{\text{Graphene}} = 11.05\ k_B T$ which are consistent with the results in Fig. 6b. The permeation rates through

various pores (Mo-only > Mixed > S-only > Graphene) can also be explained by the energy barrier that a water molecule needs to overcome to enter the pore.

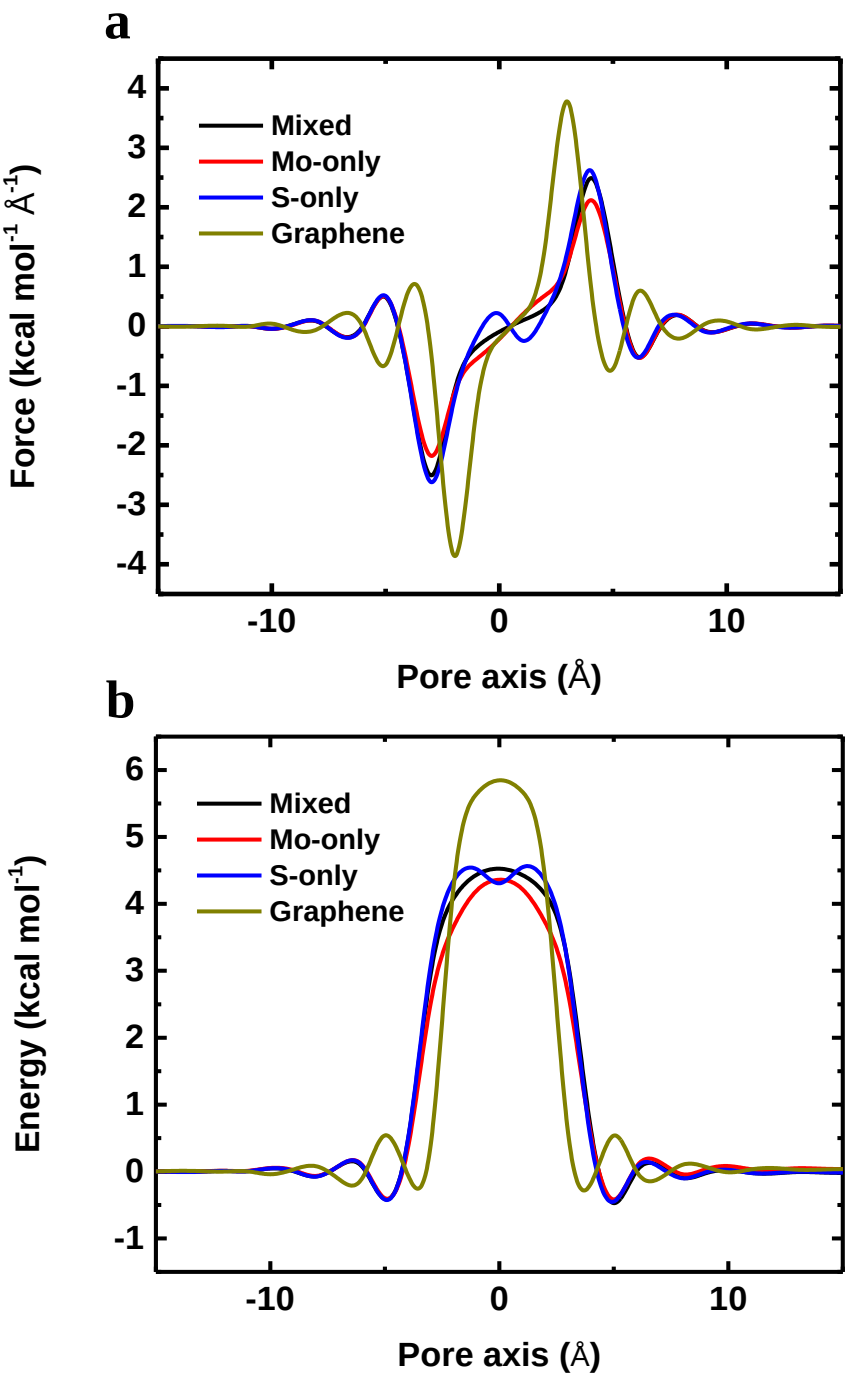

Figure 6 | (**a**) Average force on a water molecule computed along the pore axis for the Mixed, Mo-only, S-only and graphene membranes with similar pore areas. (**b**) Potential of mean force computed along the pore axis for the Mixed, Mo-only, S-only and graphene membranes with similar pore areas.

3.5 Physical Chemistry and Geometry of the Pore

Water flux (Q) is a function of density (ρ) inside the pore, velocity (V) of water through the pore and the area of the pore (A), ($Q = \rho \cdot V \cdot A$). In water desalination, increasing the area of the pore limits the salt rejection capability of the pore. As the area of the pore increases, the efficiency of rejection decreases,[25] leaving ρ and V as the control parameters to increase water flux through the pore.

As shown above, Mo-only pore exhibits the highest rate of water permeation. This can be explained by the higher water density (ρ) and velocity (V) in the Mo-only pore compared to those of the S-only and Mixed pores (Fig. 7a, Fig. 7b and Fig. 7c). The average density of water follows the order of Mo-only>Mixed> S-only (1.47 g cm^{-3}, 1.37 g cm^{-3} and 1.31 g cm^{-3}, respectively). The denser packing of water molecules at the Mo-only pore can be attributed to the hydrophilic nature of Mo sites[51] at the edge of the nanopore, which attracts water molecules to the pore interior. It has been shown that Molybdenum surface has a water contact angle close to 0° (Molybdenum is a transition metal with a large atomic diameter).[51] Attraction of water molecules toward Mo sites becomes more obvious by comparing the Mixed and S-only pores densities (Fig. 7a). In the Mixed pore, the existence of 50% Mo sites gives rise to higher density in the center of the pore compared to that of S-only pore (Fig. 7a).

Next, we explored the velocity profiles in the pore for all the three different pores. The velocities are also higher in Mo-only pores compared to Mixed and S-only pores (Fig. 7c). The average velocity of water is 8.26 m s^{-1}, 7.53 m s^{-1} and 7.51 m s^{-1} for Mo-only, Mixed and S-only pores, respectively.

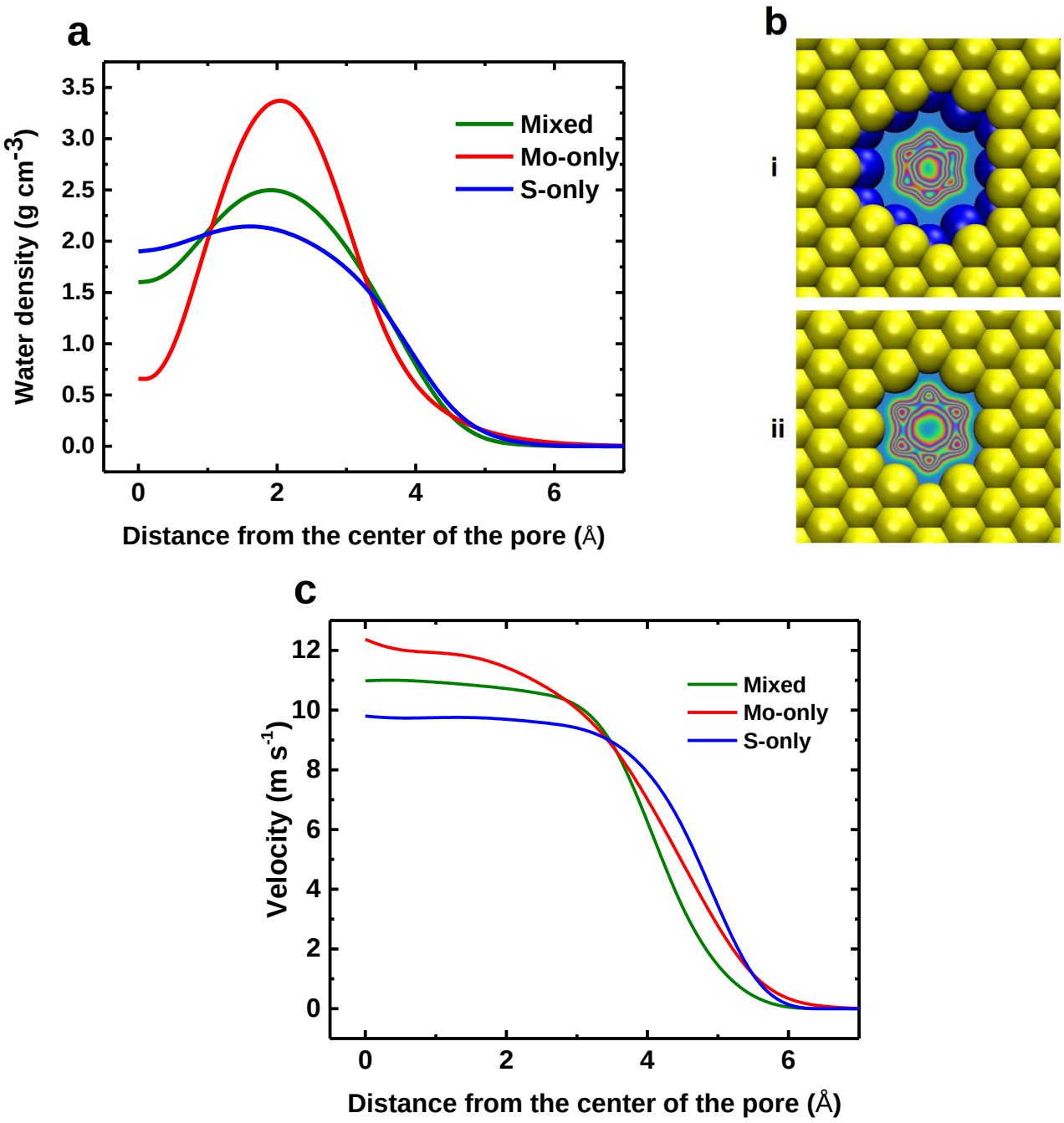

Figure 7 | (**a**) Water density distribution in the radial direction in the Mixed, Mo-only and S-only pores with equivalent pore sizes (Mixed, A=55.45 Å^2, Mo-only, A=56.42 Å^2, S-only, A=57.38 Å^2) at a fixed pressure of 250 MPa. (**b**) Density map of water distribution in Mo-only (i) and S-only (ii) pores. Blue denotes a zero probability of finding a water molecule and red indicates the highest probability of observing a water molecule. (**c**) Axial velocity of water molecules in the radial direction for Mixed, Mo-only and S-only nanopores.

To shed deeper insight into the physical understanding of why the velocity of Mo-only pore is higher compared to Mixed and S-only pores, we computed velocity profiles at the sites of S and Mo for both pore types of Mo-only and S-only (Fig. 8a and Fig. 8b).

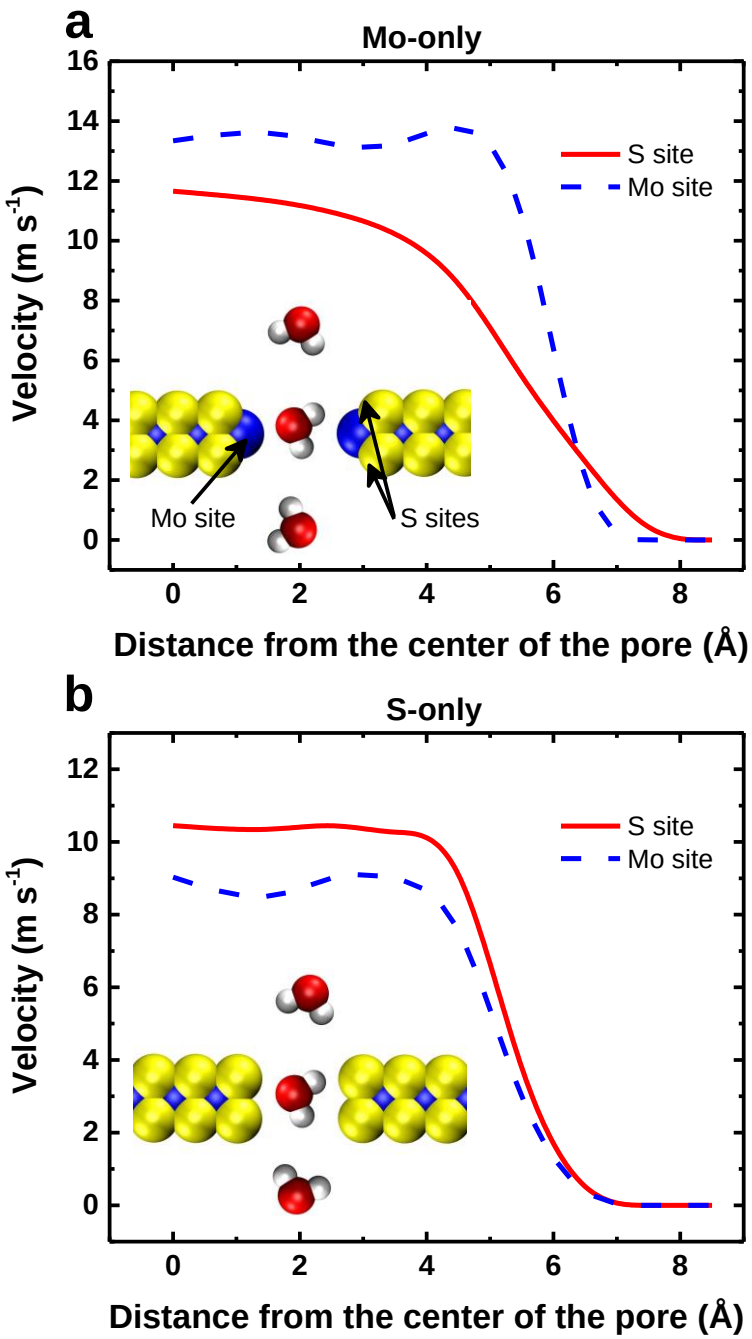

Figure 8 | (**a**) Axial velocity of water molecules in the radial direction at the location of S and Mo atom layers in the Mo-only nanopore of A=56.42 Å^2 at 250 MPa. (**b**) Axial velocity of water molecules in the radial direction at the location of S and Mo atom layers in the S-only nanopore of A=57.38 Å^2 at 250 MPa.

This is achieved by binning both pore types at Mo and S sites and averaging velocity at each point for a large number of sets of simulations. We observed that in the Mo-only pore, the velocity is higher at Mo site compared to the S sites. Unlike Mo-only pore, we did not observe the velocities to be higher in Mo site in the S-only pore, (Fig. 8a and Fig. 8b) which implies that the arrangement of Mo and S sites matter for velocity profiles. To further confirm the importance of the pore geometry in achieving the higher water velocities, the role of the atom type (Mo or S) is excluded by replacing all S atoms by Mo atoms (leading to a fictitious three-layer molybdenum membrane) as shown in Fig. 9. The axial velocities of water in the radial direction at the location of each atom layer (the middle layer of Mo, and outer layers of Mo (S layers in real MoS_2)) are plotted in Fig. 9a and Fig. 9b for both Mo-only and S-only pore structures, respectively. Comparing these velocity profiles with those of the real MoS_2, in Fig. 8, we notice that the general shape of the velocity profiles are identical meaning that the water flux is enhanced due to the nozzle-like geometry (hourglass shape) of the Mo-only pore and remains almost independent of the atom types.

It has been shown that conical nanopores have higher fluxes and permeation rates.[25,52,53] Many biological nanopores, including aquaporin[25,54,55] have an hourglass shape which facilitates rapid water permeation.[56] Solid-state nanopores have also been designed for conical/hourglass shape to enhance solute and DNA transport.[57,58] Here, in Mo-only pores, due to the fish-bone structure of MoS_2,[9] the pore can be tailored[13,27] to an hourglass shape at sub-nanometer length scale (see cartoon representation of comparison between Mo-only, S-only and graphene pores in Fig. 10). Mo-only pore has a contraction center with hydrophobic S sites at the entrance and S-only pore has an expanding center (Fig. 10). Graphene has a flat entrance and exit geometry with a single–atom type exposure at the pore surface.[43] Water molecules slip on the hydrophobic edges of S and are attracted by the hydrophilic sites of Mo at the pore center in Mo-only case.

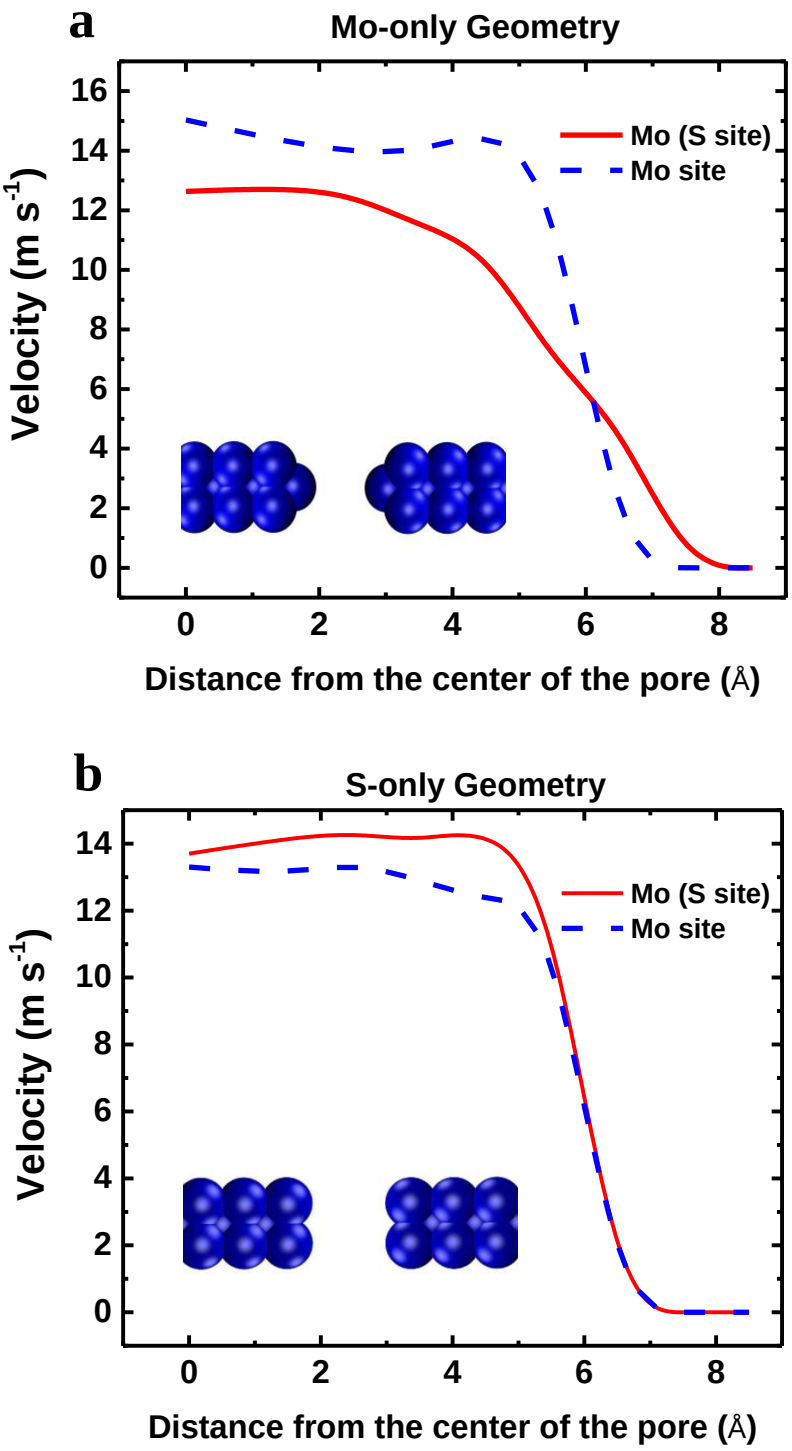

Figure 9 | Axial velocity profile of water molecules in the radial direction at the location of S and Mo atom layers where S atoms are replaced by Mo atoms (all Mo atoms). (**a**) For the Mo-only nanopore of Fig. 8a in the manuscript. (**b**) For the S-only nanopore of Fig. 8b.

This arrangement of hydrophobic and hydrophilic atoms along with the conical shape of the pore enhances the flux of water. Also, the water flux highly correlates with the energy barrier of each pore type. The computed potential of mean force (PMF) for water molecules in each pore type is the reflection of pore chemistry and geometry. In Mo-only pore, the PMF is the lowest because of the conical/hourglass and the hydrophobic-hydrophilic arrangement of the pore atoms (see Fig. 6). The fundamental advantage of Mo-only pore architecture over other pores is the interplay of geometry and chemistry to produce a higher flux of water.

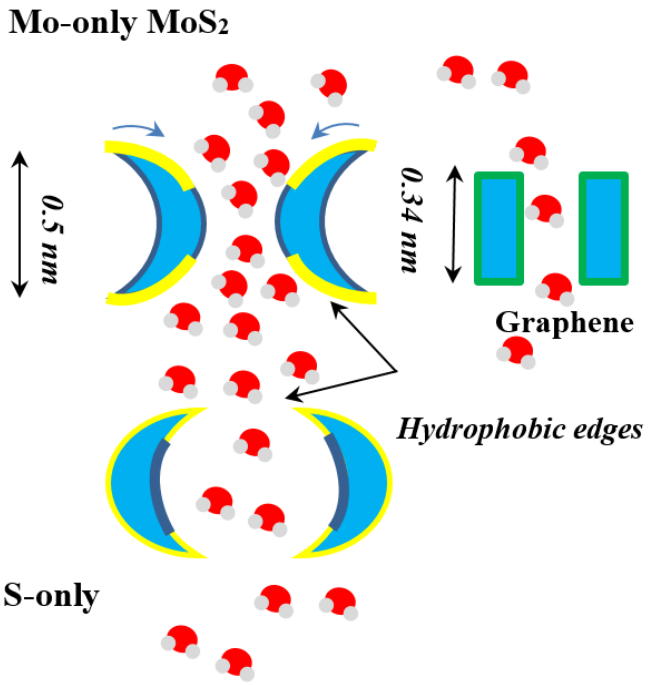

Figure 10 | Cartoon representation of the pore architecture for Mo-only, S-only and graphene nanopore.

3.6 Other Transition Metal Dichalcogenide Membranes

The molecular dynamics forcefield parameters are not available for the other transition metal dichalcogenide materials (TMD). Therefore, we swept over the Lennard-Jones parameters (σ, ε) of MoS_2 to investigate the potential performance of other TMD materials. Two different types of materials (MoX_2 and YS_2) were considered. For the MoX_2, only the parameters of the chalcogen atom (X) were varied to resemble the possible properties of membranes like $MoSe_2$ and $MoTe_2$. The Mo-only pore geometry was used and a pressure of 250 MPa was applied. As shown in Fig. 11 (part a, b and c), the water permeation rate does not change significantly with varying σ and ε of X. Since atomic size of sulfur is smaller than those of the other chalcogen atoms (Se, Te, etc.), only higher values of σ were considered.

For the other type, YS_2, the ε of the transition metal (Y) atom was varied to study the efficiency of YS_2 membranes (Fig. 11d). We did not change σ, since the pore area changes for Mo-only pore geometry. As shown in Fig. 11d, changing the parameter of Y effects the permeation rate of water which decreases with increasing ε. The ion rejection percentages of MoX_2 and YS_2 do not change significantly and lie within 3% of ion rejection of MoS_2 (92%). Based on the analysis, we conclude that the transition metal atom plays a more important role than the chalcogen atom when it comes to choosing the best TMD material for desalination.

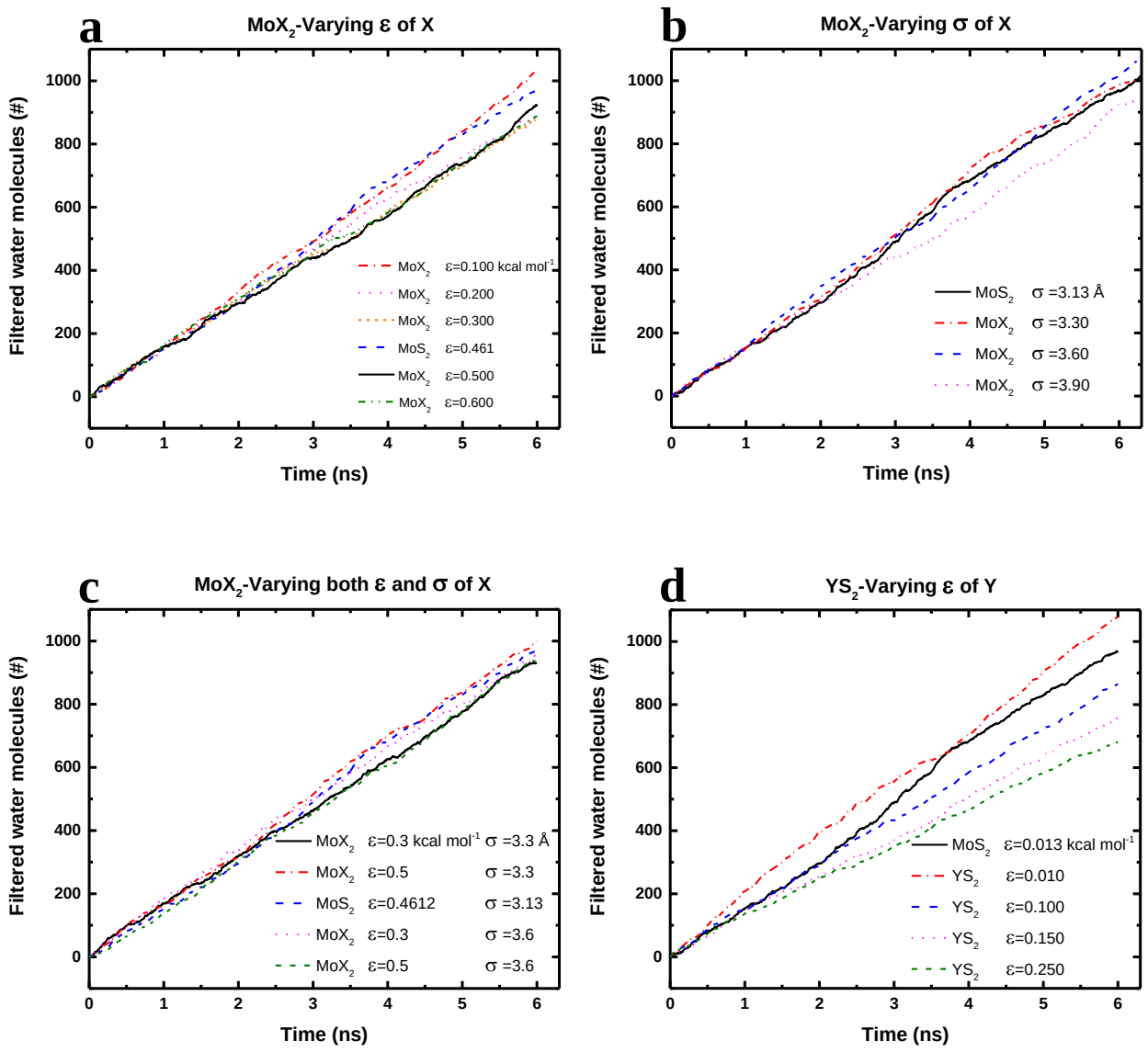

Figure 11 | Water permeation across a Mo-only geometry pore at 250 MPa for (**a**) MoX_2 by varying ε of X (**b**) MoX_2 by varying σ of X (**c**) MoX_2 by varying both ε and σ of X (**d**) YS_2 by varying ε of Y.

CHAPTER 4

DISCUSSION

Ion rejection and water flux are two important factors defining the effectiveness and performance of a water desalination membrane. In Fig. 12, ion rejection and water permeation rate are plotted for various nano-membrane materials[59] (MFI-type zeolite,[60] commercial polymeric seawater RO,[61] brackish RO,[61] Nanofiltration[61] and High-flux RO[61]) including MoS_2 and graphene investigated in this work. As shown in Fig. 12, water permeation rate is theoretically enhanced by 5 orders of magnitude using MoS_2 compared to conventional MFI-type zeolite. Also, there is a 70% improvement in the permeation rate of MoS_2 compared to graphene.

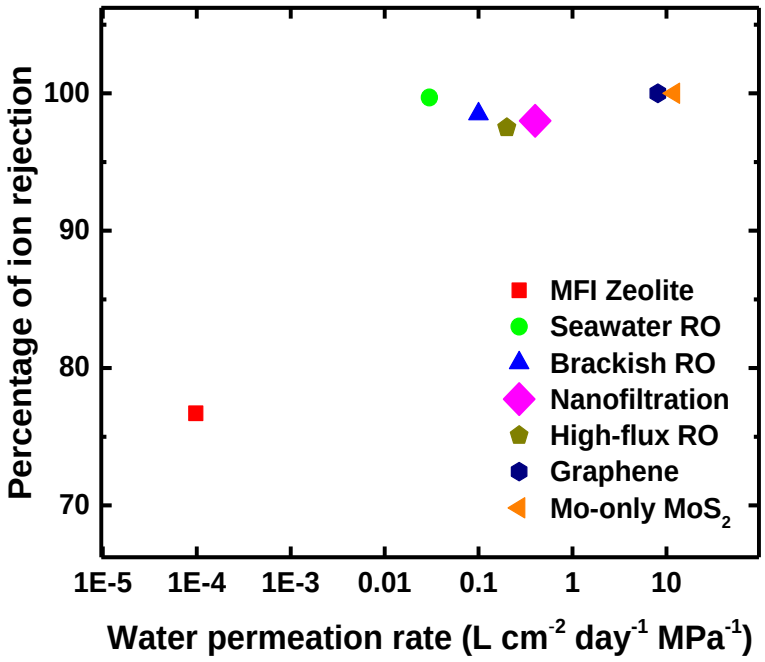

Figure 12 | Performance of membranes in terms of their ion rejection and water permeation rate. Water permeation rate is expressed per unit area of the membrane and per unit pressure as L cm^{-2} day^{-1} MPa^{-1}.

In the study by Cohen-Tanugi *et al*.,[19] the permeation rate for graphene is shown to be higher than the rate we observed for graphene. This is because, in our simulations, the porosity (the ratio of the pore area to the membrane area) is smaller which decreases the permeation rate per unit area of the membrane. In this work, the comparison of MoS_2 and graphene is performed by keeping all conditions identical in the simulations. Thus, MoS_2 is potentially an efficient membrane for water desalination.

CHAPTER 5

CONCLUSIONS

We have shown that MoS_2 membranes are promising for water purification and salt rejection. Mo-only pores perform the best among all possible MoS_2 pore architectures. MoS_2 nanopores with water accessible pore areas ranging from 20 to 60 $Å^2$ strongly reject ions allowing less than 12% of the ions (depending on pore areas) to pass through the porous membranes even at theoretically high pressures of 350 MPa. The water permeation rates associated with these MoS_2 porous membranes are found to be 2 to 5 orders of magnitude greater than that of currently used membrane materials (MFI-type zeolite, commercial polymeric seawater RO, brackish RO, Nanofiltration and High-flux RO) and 70% better than the graphene nanopore. The fish-bone, hourglass architecture of Mo-only pore with special arrangement of hydrophobic edges and hydrophilic center within 1 nm length, enhances water permeation to a large extent compared to its other counterparts.

REFERENCES

1 Elimelech, M. & Phillip, W. A. The future of seawater desalination: energy, technology, and the environment. *Science* **333**, 712-717 (2011).

2 Zhao, S. F., Zou, L., Tang, C. Y. Y. & Mulcahy, D. Recent developments in forward osmosis: opportunities and challenges. *J. Membr. Sci.* **396**, 1-21 (2012).

3 Shannon, M. A. *et al.* Science and technology for water purification in the coming decades. *Nature* **452**, 301-310 (2008).

4 Fritzmann, C., Lowenberg, J., Wintgens, T. & Melin, T. State-of-the-art of reverse osmosis desalination. *Desalination* **216**, 1-76 (2007).

5 Khawaji, A. D., Kutubkhanah, I. K. & Wie, J. M. Advances in seawater desalination technologies. *Desalination* **221**, 47-69 (2008).

6 Humplik, T. *et al.* Nanostructured materials for water desalination. *Nanotechnology* **22**, 292001 (2011).

7 Geise, G. M. *et al.* Water purification by membranes: the role of polymer science. *J. Polym. Sci. Pt. B-Polym. Phys.* **48**, 1685-1718 (2010).

8 Lee, K. P., Arnot, T. C. & Mattia, D. A review of reverse osmosis membrane materials for desalination-development to date and future potential. *J. Membr. Sci.* **370**, 1-22 (2011).

9 Liu, K., Feng, J. D., Kis, A. & Radenovic, A. Atomically thin molybdenum disulfide nanopores with high sensitivity for DNA translocation. *ACS Nano* **8**, 2504-2511 (2014).

10 Fornasiero, F. *et al.* Ion exclusion by sub-2-nm carbon nanotube pores. *Proc. Natl. Acad. Sci. U. S. A.* **105**, 17250-17255 (2008).

11 Suk, M. E. & Aluru, N. R. Water transport through ultrathin graphene. *J. Phys. Chem. Lett.* **1**, 1590-1594 (2010).

12 O'Hern, S. C. *et al.* Selective molecular transport through intrinsic defects in a single layer of CVD graphene. *ACS Nano* **6**, 10130-10138 (2012).

13 Zhao, Y. D. *et al.* Two-dimensional material membranes: an emerging platform for controllable mass transport applications. *Small* **10**, 4521-4542 (2014).

14 Zhang, D. S. *et al.* Enhanced capacitive deionization performance of graphene/carbon nanotube composites. *J. Mater. Chem.* **22**, 14696-14704 (2012).

15 Mishra, A. K. & Ramaprabhu, S. Functionalized graphene sheets for arsenic removal and desalination of sea water. *Desalination* **282**, 39-45 (2011).

16 Celebi, K. *et al.* Ultimate permeation across atomically thin porous graphene. *Science* **344**, 289-292 (2014).

17 Joseph, S. & Aluru, N. R. Why are carbon nanotubes fast transporters of water? *Nano Lett.* **8**, 452-458 (2008).

18 Suk, M. E., Raghunathan, A. V. & Aluru, N. R. Fast reverse osmosis using boron nitride and carbon nanotubes. *Appl. Phys. Lett.* **92**, 133120 (2008).

19 Cohen-Tanugi, D. & Grossman, J. C. Water desalination across nanoporous graphene. *Nano Lett.* **12**, 3602-3608 (2012).

20 Sint, K., Wang, B. & Kral, P. Selective ion passage through functionalized graphene nanopores. *J. Am. Chem. Soc.* **130**, 16448-16449 (2008).

21 Tang, Q., Zhou, Z. & Chen, Z. F. Graphene-related nanomaterials: tuning properties by functionalization. *Nanoscale* **5**, 4541-4583 (2013).

22 Farimani, A. B., Min, K. & Aluru, N. R. DNA base detection using a single-layer MoS_2. *ACS Nano* **8**, 7914-7922 (2014).

23 Radisavljevic, B., Radenovic, A., Brivio, J., Giacometti, V. & Kis, A. Single-layer MoS_2 transistors. *Nat. Nanotechnol.* **6**, 147-150 (2011).

24 Bertolazzi, S., Brivio, J. & Kis, A. Stretching and breaking of ultrathin MoS_2. *ACS Nano* **5**, 9703-9709 (2011).

25 Gravelle, S. *et al.* Optimizing water permeability through the hourglass shape of aquaporins. *Proc. Natl. Acad. Sci. U. S. A.* **110**, 16367-16372 (2013).

26 Waduge, P. *et al.* Direct and scalable deposition of atomically thin low-noise MoS_2 membranes on apertures. *ACS Nano* **9**, 7352-7359 (2015).

27 Feng, J. *et al.* Electrochemical reaction in single layer MoS_2: nanopores opened atom by atom. *Nano Lett.* **15**, 3431-3438 (2015).

28 Lee, Y. H. *et al.* Synthesis of large-area MoS_2 atomic layers with chemical vapor deposition. *Adv. Mater.* **24**, 2320-2325 (2012).

29 Dumcenco, D. *et al.* Large-area epitaxial monolayer MoS_2. *ACS Nano* **9**, 4611-4620 (2015).

30 Coleman, J. N. *et al.* Two-dimensional nanosheets produced by liquid exfoliation of layered materials. *Science* **331**, 568-571 (2011).

31 Smith, R. J. *et al.* Large-scale exfoliation of inorganic layered compounds in aqueous surfactant solutions. *Adv. Mater.* **23**, 3944-3948 (2011).

32 Liu, K. K. *et al.* Growth of large-area and highly crystalline MoS_2 thin layers on insulating substrates. *Nano Lett.* **12**, 1538-1544 (2012).

33 Zhan, Y. J., Liu, Z., Najmaei, S., Ajayan, P. M. & Lou, J. Large-area vapor-phase growth and characterization of MoS_2 atomic layers on a SiO_2 substrate. *Small* **8**, 966-971 (2012).

34 Jeon, J. *et al.* Layer-controlled CVD growth of large-area two-dimensional MoS_2 films. *Nanoscale* **7**, 1688-1695 (2015).

35 Mann, J. *et al.* 2-dimensional transition metal dichalcogenides with tunable direct band gaps: $MoS_{2(1-x)}Se_{2x}$ monolayers. *Adv. Mater.* **26**, 1399-1404 (2014).

36 van der Zande, A. M. *et al.* Grains and grain boundaries in highly crystalline monolayer molybdenum disulphide. *Nat. Mater.* **12**, 554-561 (2013).

37 Yu, Y. F. *et al.* Controlled scalable synthesis of uniform, high-quality monolayer and few-layer MoS_2 films. *Sci. Rep.* **3**, 6 (2013).

38 Plimpton, S. Fast parallel algorithms for short-range molecular-dynamics. *J. Comput. Phys.* **117**, 1-19 (1995).

39 Humphrey, W., Dalke, A. & Schulten, K. VMD: Visual molecular dynamics. *J. Mol. Graph.* **14**, 33-38 (1996).

40 Hockney, R. W. & Eastwood, J. W. *Computer simulation using particles*. (Taylor & Francis, Inc., 1988).

41 Nose, S. A unified formulation of the constant temperature molecular-dynamics methods. *J. Chem. Phys.* **81**, 511-519 (1984).

42 Hoover, W. G. Canonical dynamics-equilibrium phase-space distributions. *Phys. Rev. A* **31**, 1695-1697 (1985).

43 Wu, Y. B. & Aluru, N. R. Graphitic carbon-water nonbonded interaction parameters. *J. Phys. Chem. B* **117**, 8802-8813 (2013).

44 Farimani, A. B. & Aluru, N. R. Spatial diffusion of water in carbon nanotubes: from fickian to ballistic motion. *J. Phys. Chem. B* **115**, 12145-12149 (2011).

45 Liang, T., Phillpot, S. R. & Sinnott, S. B. Parametrization of a reactive many-body potential for Mo-S systems. *Phys. Rev. B* **79**, 245110 (2009).

46 Joung, I. S. & Cheatham, T. E. Determination of alkali and halide monovalent ion parameters for use in explicitly solvated biomolecular simulations. *J. Phys. Chem. B* **112**, 9020-9041 (2008).

47 Mizan, T. I., Savage, P. E. & Ziff, R. M. Molecular-dynamics of supercritical water using a flexible spc model. *J. Phys. Chem.* **98**, 13067-13076 (1994).

48 Rosenberg, P. A. & Finkelstein, A. Water permeability of gramicidin-a-treated lipid bilayer membranes. *J. Gen. Physiol.* **72**, 341-350 (1978).

49 Suk, M. E. & Aluru, N. R. Effect of induced electric field on single-file reverse osmosis. *Phys. Chem. Chem. Phys.* **11**, 8614-8619 (2009).

50 Zhu, F. Q., Tajkhorshid, E. & Schulten, K. Pressure-induced water transport in membrane channels studied by molecular dynamics. *Biophys. J.* **83**, 154-160 (2002).

51 Liu, Y. H. *et al.* The preparation of a strawberry-like super-hydrophilic surface on the molybdenum substrate. *Colloid Surf. A-Physicochem. Eng. Asp.* **404**, 52-55 (2012).

52 Gravelle, S., Joly, L., Ybert, C. & Bocquet, L. Large permeabilities of hourglass nanopores: from hydrodynamics to single file transport. *J. Chem. Phys.* **141**, 18C526 (2014).

53 Bocquet, L. & Tabeling, P. Physics and technological aspects of nanofluidics. *Lab Chip* **14**, 3143-3158 (2014).

54 Farimani, A. B., Aluru, N. R. & Tajkhorshid, E. Thermodynamic insight into spontaneous hydration and rapid water permeation in aquaporins. *Appl. Phys. Lett.* **105**, 83702-83702 (2014).

55 Jung, J. S., Preston, G. M., Smith, B. L., Guggino, W. B. & Agre, P. Molecular-structure of the water channel through aquaporin chip - the hourglass model. *J. Biol. Chem.* **269**, 14648-14654 (1994).

56 Hou, X., Guo, W. & Jiang, L. Biomimetic smart nanopores and nanochannels. *Chem. Soc. Rev.* **40**, 2385-2401 (2011).

57 Dekker, C. Solid-state nanopores. *Nat. Nanotechnol.* **2**, 209-215 (2007).

58 Heins, E. A., Siwy, Z. S., Baker, L. A. & Martin, C. R. Detecting single porphyrin molecules in a conically shaped synthetic nanopore. *Nano Lett.* **5**, 1824-1829 (2005).

59 Pendergast, M. M. & Hoek, E. M. V. A review of water treatment membrane nanotechnologies. *Energy Environ. Sci.* **4**, 1946-1971 (2011).

60 Li, L. X., Dong, J. H., Nenoff, T. M. & Lee, R. Desalination by reverse osmosis using MFI zeolite membranes. *J. Membr. Sci.* **243**, 401-404 (2004).

61 Guillen, G. & Hoek, E. M. V. Modeling the impacts of feed spacer geometry on reverse osmosis and nanofiltration processes. *Chem. Eng. J.* **149**, 221-231 (2009).